J. Fluid Mech. (2015), *vol.* 779, *pp.* 371–389.
doi:10.1017/jfm.2015.273

Turbulent boundary layer statistics at very high Reynolds number

M. Vallikivi[1], M. Hultmark[1,†] and A. J. Smits[1,2]

[1]Department of Mechanical and Aerospace Engineering, Princeton University, Princeton, NJ 08544, USA

[2]Department of Mechanical and Aerospace Engineering, Monash University, Melbourne, VIC 3800, Australia

(Received 10 June 2014; revised 14 January 2015; accepted 7 May 2015; first published online 17 August 2015)

Measurements are presented in zero-pressure-gradient, flat-plate, turbulent boundary layers for Reynolds numbers ranging from $Re_\tau = 2600$ to $Re_\tau = 72\,500$ ($Re_\theta = 8400$–$235\,000$). The wind tunnel facility uses pressurized air as the working fluid, and in combination with MEMS-based sensors to resolve the small scales of motion allows for a unique investigation of boundary layer flow at very high Reynolds numbers. The data include mean velocities, streamwise turbulence variances, and moments up to 10th order. The results are compared to previously reported high Reynolds number pipe flow data. For $Re_\tau \geqslant 20\,000$, both flows display a logarithmic region in the profiles of the mean velocity and all even moments, suggesting the emergence of a universal behaviour in the statistics at these high Reynolds numbers.

Key words: turbulent boundary layers, turbulent flows

1. Introduction

The scaling of turbulent wall-bounded flows with Reynolds number has been the subject of much recent interest and debate (Marusic *et al.* 2010; Smits, McKeon & Marusic 2011*a*; Smits & Marusic 2013), and new experiments have expanded considerably the range of Reynolds numbers available for study. For example, examinations of pipe flow have reported mean flow data at values of Re_τ as high as 530 000 (Zagarola & Smits 1998; McKeon *et al.* 2004), where Re_τ is the friction Reynolds number, with turbulence data at values up to 98 000 (Hultmark *et al.* 2012, 2013; Rosenberg *et al.* 2013). For boundary layer flows under laboratory conditions, the corresponding values are 70 000 (Winter & Gaudet 1973) and 19 000 (Mathis, Hutchins & Marusic 2009), although some limited but valuable turbulence data were acquired at 69 000 in the LCC facility by Winkel *et al.* (2012), and at 650 000 in the neutral atmospheric boundary layer by Hutchins *et al.* (2012).

The available laboratory data are limited in Reynolds number primarily because of experimental difficulties. Conducting high Reynolds number experiments usually requires large and often expensive facilities, and for scaling studies the flows need to be of high quality and employ high-resolution instrumentation. Here, we use a pressurized facility, the Princeton High Reynolds Number Test Facility (HRTF), to

† Email address for correspondence: hultmark@princeton.edu

generate very high Reynolds number flat-plate boundary layers. We report results obtained at a maximum Reynolds number based on the momentum thickness of 235 000, which is believed to be higher than that investigated in any previous laboratory study featuring well-controlled initial and boundary conditions. The HRTF is the counterpart to the Princeton Superpipe facility, which has been extensively used to examine very high Reynolds number pipe flows. Here, we present the first data from this unique boundary layer wind tunnel, which, together with novel nanoscale flow sensors, will enable us to investigate canonical flat-plate boundary layers over an unprecedented range of Reynolds numbers.

The friction Reynolds number, $Re_\tau = u_\tau \delta/\nu$, provides a common standard for comparisons among wall-bounded flows. Here, $u_\tau = \sqrt{\tau_w/\rho}$ is the friction velocity, τ_w is the wall shear stress, ρ and ν are fluid density and kinematic viscosity, respectively, and δ is the boundary layer thickness δ_{99}, or the pipe radius R, or the half-height of the channel h. This Reynolds number, also known as the von Kármán number, characterizes the range of scales present in the flow, and avoids the use of more specific velocity and length scales such as the free-stream velocity U_∞, the bulk velocity $\langle U \rangle$, the momentum thickness θ, or the displacement thickness δ^*.

For turbulent wall-bounded flows at sufficiently large Reynolds numbers, we expect that for $y^+ = yu_\tau/\nu \gg 1$ and $y/\delta \ll 1$, the mean velocity U behaves logarithmically according to

$$U^+ = \frac{1}{\kappa} \ln y^+ + B \tag{1.1}$$

(Millikan 1938), where $U^+ = U/u_\tau$, y is the wall-normal distance, κ is the von Kármán constant, and B is the additive constant for the mean velocity. The values of κ reported in the past have varied over a considerable range, with values as low as 0.38 in a boundary layer (Österlund *et al.* 2000) and as high as 0.42 in a pipe (McKeon *et al.* 2004). A recent study by Bailey *et al.* (2014) showed that for pipe flow $\kappa = 0.40 \pm 0.02$, where the uncertainty estimate reflects the many sources of error that make it difficult to find κ more precisely even when the friction velocity is well known. For boundary layers one would expect an even larger variation due to the difficulty in estimating u_τ.

The pipe flow measurements by Zagarola & Smits (1998) and McKeon *et al.* (2004) revealed that the start of the log-law region in the mean flow, commonly assumed to be located at $y^+ = 30$–50, was actually located much further from the wall at $y^+ = 600$, or even $y^+ = 1000$. In boundary layers, George & Castillo (1997) argued that the inner limit was located at $y^+ \approx 300$, whereas Wei *et al.* (2005) suggested a Reynolds-number-dependent lower limit and Nagib, Chauhan & Monkewitz (2007) reported a value of $y^+ = 200$. As to the outer limit, values in the literature range from $y/\delta = 0.08$ to 0.3, with Marusic *et al.* (2013) suggesting a value of 0.15. With an inner limit of $y^+ = 300$, and an outer limit of $y/\delta = 0.15$, a decade of logarithmic variation in the mean velocity of a boundary layer is not expected to occur until $Re_\tau = 20\,000$, which is the upper limit of the detailed data sets that have so far been available for boundary layers.

As to the behaviour of the turbulence, Townsend (1976) and Perry, Henbest & Chong (1986) suggested that a logarithmic behaviour in streamwise and wall-parallel fluctuations should also occur in the region where (1.1) holds, if the Reynolds number is large enough. That is, for the streamwise velocity fluctuations u, we would expect

$$u^{2+} = B_1 - A_1 \ln \frac{y}{\delta}, \tag{1.2}$$

where $u^{2+} = \overline{u^2}/u_\tau^2$, A_1 is the Townsend–Perry constant, and B_1 is the additive constant for the variance. This logarithmic behaviour was first observed experimentally in pipe flow over a significant wall-normal extent by Hultmark *et al.* (2012), where it only became evident for $y/R < 0.12$ once $Re_\tau \geqslant 20\,000$, with a spatial extent that increased with Reynolds number. Marusic *et al.* (2013) suggested that this scaling also applies in boundary layers, and proposed a universal value of $A_1 = 1.26$.

In deriving (1.2), Townsend appealed to his attached eddy hypothesis, where the turbulent eddy length scales are assumed to be proportional to y with a population density proportional to y^{-1}. Meneveau & Marusic (2013) used this hypothesis to show that if the summands are assumed to be statistically independent (as in the case of non-interacting eddies), the pth root of moments of velocity fluctuations is expected to behave according to

$$\langle (u^+)^{2p} \rangle^{1/p} = B_p - A_p \ln \frac{y}{\delta}, \tag{1.3}$$

where A_p and B_p are constants, at least at fixed Reynolds number. They examined the validity of this generalized logarithmic law in boundary layers with Re_τ up to 19 000, and found that the behaviour of high-order moments was sub-Gaussian, and that there may be a universal value of A_p.

It is evident from this previous work that high Reynolds number data reveal intriguing trends in the scaling of the mean flow and the turbulence. At the same time it is clear that for boundary layers high-quality turbulence data over any extensive range of Reynolds numbers is limited to values of $Re_\tau < 20\,000$, and it appears that this might be the lower limit of what is possibly the start of an asymptotic behaviour (Smits & Marusic 2013). In order to extend the boundary layer observations beyond this value, we now describe a new experimental study that examines turbulent boundary layer behaviour for $2600 \leqslant Re_\tau \leqslant 72\,500$. Here, we focus on the behaviour of the mean flow, the variance, and the higher-order moments of the streamwise velocity fluctuations. The spectral behaviour is reported separately by Vallikivi, Ganapathisubramani & Smits (2015). We will, wherever possible, compare the boundary layer data with the results of pipe flow at similar Reynolds numbers.

2. Experimental methods

The measurements were conducted in the HRTF at the Princeton University Gas Dynamics Laboratory. The HRTF is a closed-loop wind tunnel that uses air at pressures up to 220 atm as the working fluid. The tunnel has a maximum speed of 12 m s^{-1} and free-stream turbulence intensity levels between 0.3 and 0.6 %. It has two working sections, each 2.44 m long with a 0.49 m inner diameter, as shown in figure 1(*a*). The facility is described in further detail by Jiménez, Hultmark & Smits (2010).

A 2.06 m flat-plate model with an elliptic leading edge was mounted in the downstream test section of the wind tunnel. A 1 mm square tripwire, located 76 mm from the leading edge, was used to trip the boundary layer. A single measurement station was used, located 1.82 m downstream of the tripwire (figure 1*b*). The aluminum surface of the plate was polished to a mirror finish. The surface roughness was estimated using an optical microscope and comparator plates and found to be less than 0.15 μm, corresponding to $k_{rms}^+ < 0.4$ at the highest Reynolds number studied, so that for all conditions the plate was assumed to be hydraulically smooth.

The pressure distribution in the circular test section was adjusted using a 'blister' insert attached to the tunnel wall on the opposite side of the plate, as shown

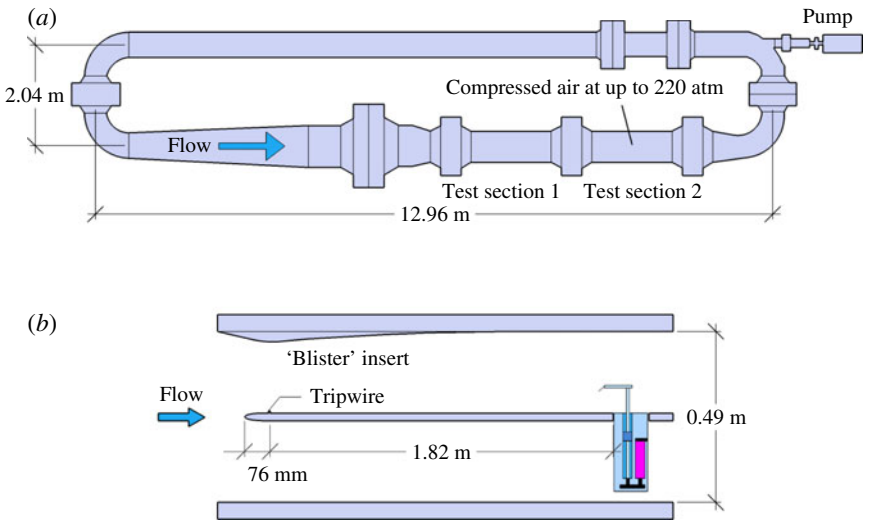

FIGURE 1. (Colour online) The Princeton HRTF. (*a*) Tunnel layout; (*b*) flat-plate details.

in figure 1(*b*). The pressure distribution was measured using 18 streamwise and 15 spanwise pressure taps, and the insert was adjusted to minimize the pressure gradient. The local streamwise pressure gradient parameter $K_p = (\nu/U_\infty^2)(\mathrm{d}U_\infty/\mathrm{d}x) = (\nu/\rho u_\tau^3)(\mathrm{d}p/\mathrm{d}x)$ was found to be less than 1×10^{-8} for all cases (Vallikivi, Hultmark & Smits 2013; Vallikivi 2014). This value is an order of magnitude smaller than that reported in some previous studies (for example, DeGraaff & Eaton (2000) reported $K_p < 1.1 \times 10^{-7}$), and therefore the flow was assumed to be free of pressure gradient effects.

2.1. *NSTAP measurements*

In the current study, two nanoscale thermal anemometry probes (NSTAPs) were used, one with filament length $\ell = 60$ μm and cross-section 0.1 μm × 2 μm, and a second one with $\ell = 30$ μm and cross-section 0.08 μm × 1.5 μm. The fabrication, validation and behaviour of these sensors are described in detail by Bailey *et al.* (2010), Vallikivi *et al.* (2011) and Vallikivi & Smits (2014).

The sensors were operated using a Dantec Streamline Constant Temperature Anemometry system with a 1:1 bridge, keeping the heated filament at a temperature of about 450 K. The frequency response, determined from a square wave test, was always above 150 kHz in still air, increasing to more than 300 kHz in the flow. The data were digitized using a 16-bit A/D board (NI PCI-6123) at a rate of 300 kHz and low-pass filtered using an eighth-order Butterworth filter at 150 kHz. The sensor was traversed in the wall-normal direction using a stepper motor traverse with a Numeric Jena LIK22 encoder with a resolution of 0.05 μm. The initial wall-normal distance y_0 of the probe was measured using a depth-measuring microscope (Titan Tool Supply Inc.) with an accuracy of 5 μm.

The NSTAPs were calibrated using a 0.4 mm Pitot tube together with two 0.4 mm static pressure taps located in the pipe wall at the same streamwise location. The Pitot tube measurements were corrected for static tap Reynolds number effects and viscous effects using the correlations proposed by McKeon & Smits (2002) and McKeon *et al.* (2003), respectively. Fourteen calibration points were used, and the calibration was

Case	Sensor	$Re_\theta \times 10^3$	Re_τ	p_a (atm)	U_∞ (m s^{-1})	ν/u_τ (μm)	ℓ or d_p (μm)	ℓ^+ or d_p^+	y_0 (μm)	y_0^+	Symbol
1	NSTAP	8.4	2622	4.4	9.08	10	60	5.8	40	3.9	
2	NSTAP	15.1	4635	8.1	9.21	5.9	60	10	40	6.8	
3	NSTAP	26.9	8261	15	9.29	3.4	60	17	40	12	
4	NSTAP	46.7	14 717	30	9.33	1.8	60	33	40	22	
5	NSTAP	80.6	25 062	57	9.46	1.0	30	29	20	19	
6	NSTAP	113	40 053	105	9.50	0.6	30	47	20	31	
7	NSTAP	235	72 526	213	9.55	0.4	30	75	20	50	
8	Pitot	9.4	2841	4.4	9.40	10	200	20	130	13	
9	Pitot	16.0	4835	8.0	9.51	5.9	200	34	130	22	
10	Pitot	28.4	8622	15	9.61	3.4	200	59	130	38	
11	Pitot	50.7	15 256	28	9.64	1.8	200	109	130	70	
12	Pitot	90.6	26 609	57	9.53	1.0	200	197	130	126	
13	Pitot	147	43 481	107	9.58	0.6	200	329	130	211	
14	Pitot	223	65 129	214	9.55	0.4	200	506	130	324	

TABLE 1. Experimental conditions for boundary layer measurements: p_a is the ambient tunnel pressure, y_0 is the initial distance from the wall, and u_τ is derived using the correlation proposed by Fernholz & Finley (1996). Cases 1–7: NSTAP data with sensor length ℓ. Cases 8–14: Pitot probe data with diameter d_p.

performed before and after each profile measurement. A fourth-order polynomial fit was used to find the calibration coefficients. The ambient fluid temperature change during a given profile ranged from 0.7 to 10.0 °C over the full Reynolds number range, and the data were corrected using the temperature correction outlined by Hultmark & Smits (2010).

NSTAP data were acquired for $2600 < Re_\tau < 72\,500$, corresponding to $8400 < Re_\theta < 235\,000$ (where $Re_\theta = U_\infty\theta/\nu$). The tunnel was pressurized for all cases and the experimental conditions are listed in table 1 (cases 1–7). Here, p_a denotes the ambient pressure, ℓ^+ is the wire length in viscous units ($=\ell u_\tau/\nu$), y_0 is the initial wall-normal distance and $y_0^+ = y_0 u_\tau/\nu$. The data were sampled for 60 s in cases 1–6 and for 20 s in case 7, corresponding to convection lengths of more than 20 000 and 5000δ, respectively. Convergence was tested by comparing the magnitudes of the moments evaluated over the full sampling time with those obtained over half the sampling time. Even for the 10th-order moment, the differences were within 3 %.

It can be seen from table 1 that at the higher Reynolds number even the NSTAP probe has insufficient spatial resolution. To minimize bias errors due to spatial filtering, the correction by Smits *et al.* (2011*b*) was applied to the variance. Smits *et al.* showed that this correction works well for ℓ^+ up to 153, considerably greater than the maximum value found here (=75). Any data on the variance where the spatial filtering correction exceeded 5 % are shown with grey symbols in figure 4. Note that spatial resolution has its major effect in the near-wall region, and even at the highest Reynolds numbers the correction is less than 5 % for $200\nu/u_\tau < y = 0.003\delta$. For the higher-order moments, no equivalent correction method exists, so all higher-order data points where the correction on the variance exceeded 5 % were removed from the data set. In addition to spatial filtering, there is the uncertainty in initial wall location y_0 (about 5 μm), which needs to be borne in mind when examining the results for $y^+ < 100$ at high Reynolds numbers.

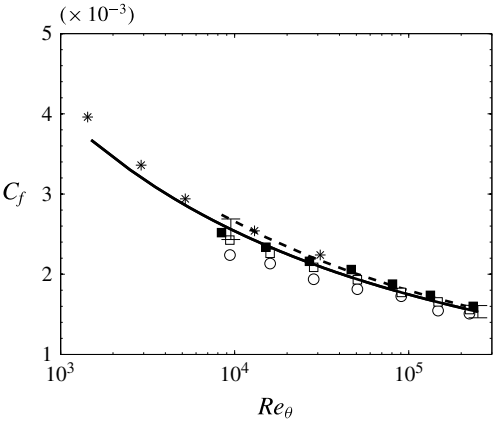

FIGURE 2. Boundary layer skin friction coefficient C_f: ○, Preston tube; □, Clauser fit for Pitot data sets; ■, Clauser fit for NSTAP data sets (Clauser 1956); ∗, DeGraaff & Eaton (2000); solid line, Fernholz & Finley (1996); dashed line, Winter & Gaudet (1973). Error bars indicate ±5 %.

2.2. *Pitot tube measurements*

In addition to the NSTAP data, Pitot tube measurements were taken for $2800 < Re_\tau < 65\,000$, corresponding to $9400 < Re_\theta < 223\,000$. The experimental conditions for these cases are given in table 1 (cases 8–14). A Pitot probe with an outer diameter of $d_p = 0.20$ mm was used, in conjunction with two 0.4 mm static pressure taps in the plate. The pressure difference was measured using a DP15 Validyne pressure transducer with a 1.40 kPa range which was calibrated against a manometer standard. As for the NSTAP measurements, the initial wall distance of the Pitot probe y_0 was measured using a depth-measuring optical microscope and the probe was traversed in the wall-normal direction using a stepper motor traverse with a resolution of 0.05 μm. The Pitot tube measurements were corrected following Bailey *et al.* (2013), including the static tap correction by McKeon *et al.* (2003), viscous and shear corrections by Zagarola & Smits (1998), and the near-wall correction by MacMillan (1957). The data for wall distances smaller than $2d_p$ were neglected, as in the pipe flow experiments described by Bailey *et al.* (2014). Further details on the experimental techniques are given by Vallikivi (2014).

2.3. *Friction velocity*

To determine u_τ and the skin friction coefficient $C_f = 2u_\tau^2/U_\infty^2$, a number of different methods were used. First, the 0.2 mm Pitot probe when in contact with the wall was used as a Preston tube (Patel 1965; Zagarola, Williams & Smits 2001). Second, the Clauser chart technique (Clauser 1956) was used, where the log-law was fitted to the velocity profiles using the constants $\kappa = 0.40$ and $B = 5.1$ recommended by Coles (1956). These results were compared to the skin friction correlation proposed by Fernholz & Finley (1996), as well as data from one of the few direct measurements of skin friction using a drag plate at high Reynolds number (Winter & Gaudet 1973) (see figure 2). For comparison, values from DeGraaff & Eaton (2000) found using the Clauser chart are also shown.

All C_f estimates except for the Preston tube data had a standard deviation less than 3 % compared to the Fernholz correlation. In addition, the Fernholz correlation closely

Case	Re_D	Re_τ	p_a (atm)	$\langle U \rangle$ (m s^{-1})	ν/u_τ (μm)	ℓ (μm)	ℓ^+	y_0 (μm)	y_0^+	Symbol
1	146×10^3	3 334	0.67	10.1	19	60	3.1	14	0.74	▽
2	247×10^3	5 412	2.40	8.40	12	60	5.0	14	1.2	□
3	512×10^3	10 481	5.43	9.37	6.2	60	9.7	14	2.3	△
4	1.1×10^6	20 250	10.8	10.5	3.2	60	18.8	14	4.4	◇
5	2.1×10^6	37 690	22.5	10.5	1.7	60	35.0	14	8.2	◁
6	4.0×10^6	68 371	45.9	10.3	0.95	30	31.7	28	29	○
7	6.0×10^6	98 190	69.7	10.6	0.66	30	45.5	28	43	☆

TABLE 2. Pipe flow data for comparison, from Hultmark *et al.* (2013).

matches the average value obtained by the other methods, and it agrees well with the force plate measurements by Winter & Gaudet (1973) over the same Reynolds number range. Hence, we used the value of u_τ determined from the Fernholz correlation for all subsequent data analysis.

2.4. *Pipe flow data for comparison*

We compare the turbulent boundary layer data with that from fully developed turbulent pipe flow obtained by Hultmark *et al.* (2012, 2013). The cases used for comparison are listed in table 2, and cover $3300 \leqslant Re_\tau \leqslant 98\,000$.

3. Results and discussion

In presenting the results, we use a single notation δ to denote the outer length scale, that is, the boundary layer thickness for boundary layer data and the pipe radius for pipe flow data.

3.1. *Mean flow*

The mean velocity profiles for the boundary layer are shown in figure 3. The agreement between the NSTAP and Pitot profiles is within 1.3 %, well within the uncertainty on U (estimated to be <2.2 %). The mean velocity behaviour and scaling in boundary layers may be compared to the behaviour in pipe flow by referring to the extensive discussions of pipe flows given by Zagarola & Smits (1998), McKeon *et al.* (2004), Hultmark *et al.* (2013) and Bailey *et al.* (2014), and so this will not be repeated here. Suffice it to say that both flows show an extended region of logarithmic behaviour, although for the boundary layer this behaviour starts closer to the wall compared to pipe flows, where the log-law only appears for $y^+ > 600$–800. The middle of the log-layer, located at $y^+ = 3Re_\tau^{0.5}$ according to Marusic *et al.* (2013), served as a conservative lower bound for fitting the logarithmic portion of the profile, and for all cases the log-layer was found to extend to about 0.15δ. Due to the many uncertainties in the evaluation of the slope (and friction velocity in the boundary layer), it is not possible to determine any differences in the von Kármán constant between pipes and boundary layers (Bailey *et al.* 2014). The constants proposed by Coles (1956) ($\kappa = 0.40$ and $B = 5.1$) give an equally good fit for both flows.

Table 3 lists the boundary layer thickness $\delta = \delta_{99}$, displacement thickness δ^*, momentum thickness θ, and shape factor $H = \delta^*/\theta$ for each case. All bulk properties were found to decrease with Reynolds number in the expected manner, as observed by DeGraaff & Eaton (2000) and others, and they are discussed in more detail by Vallikivi *et al.* (2013) and Vallikivi (2014).

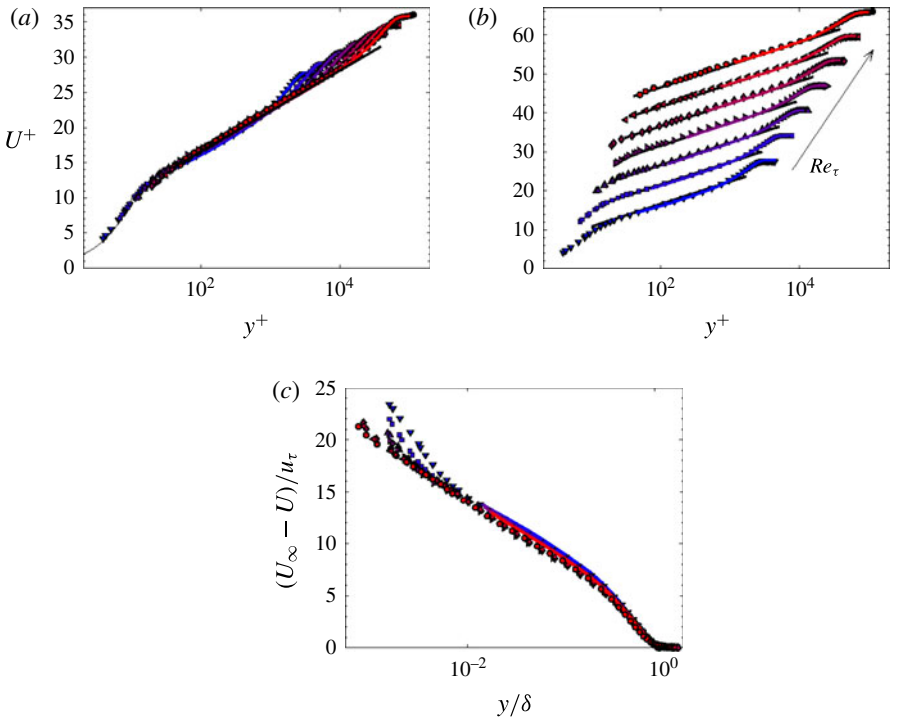

FIGURE 3. Boundary layer mean velocity profiles. (*a*) Inner coordinates; (*b*) inner coordinates, each profile shifted by $\Delta U^+ = 5$; (*c*) outer coordinates. Symbols as given in table 1. In (*a*,*b*) solid black lines show (1.1) with $\kappa = 0.40$ and $B = 5.1$; thin solid lines show $U^+ = y^+$.

3.2. *Variances*

In figure 4, profiles of the streamwise variances u^{2+} are shown in inner coordinates, with the boundary layer data on the left and the pipe flow data on the right. Points in the boundary layer data where the spatial filtering correction is greater than 5 % are indicated by grey symbols. The two flows show a broadly similar behaviour with a distinct inner peak at approximately the same wall-normal position. The inner peak appears to be invariant with Reynolds number, with a non-dimensional magnitude $u_I^{2+} = 8.4 \pm 0.8$ for the boundary layer data, which agrees with the pipe data within experimental error. However, the inner peak values for the boundary layer are only resolved for the three lowest Reynolds numbers tested ($2622 \leqslant Re_\tau \leqslant 8261$). Thus, the data cannot resolve the question regarding the scaling of the inner peak at higher Reynolds numbers.

The data indicate that an outer peak emerges at approximately the same Reynolds number for the two flows. The outer peak magnitude, u_{II}^{2+}, was found for each Reynolds number (for the three lowest Reynolds numbers there is no peak, and so the inflection point was used instead), and the results shown in figure 5 demonstrate that the magnitudes of the outer peaks are very similar in boundary layer and pipe flows.

Pullin *et al.* (2013) presented an analysis that supports a logarithmic increase in the outer peak value u_{II}^{2+} with Reynolds number, with two possible relations depending

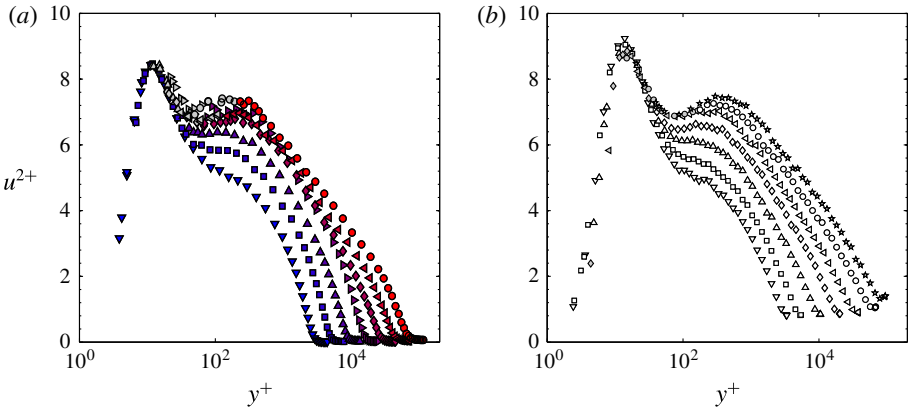

FIGURE 4. Variance profiles in inner coordinates: (*a*) boundary layer; (*b*) pipe. Symbols as given in tables 1 and 2. Grey symbols indicate boundary layer data where the spatial filtering exceeds 5 % according to the correction by Smits *et al.* (2011*b*).

Case	δ (mm)	δ^* (mm)	θ (mm)	H	$C_f \times 10^3$
1	27.2	4.24	3.15	1.34	2.62
2	27.3	4.01	3.06	1.31	2.36
3	28.4	3.89	3.02	1.29	2.14
4	27.0	3.38	2.68	1.26	1.96
5	25.7	3.09	2.49	1.24	1.80
6	25.8	3.06	2.48	1.24	1.68
7	29.1	3.20	2.62	1.22	1.55
8	28.7	4.59	3.39	1.35	2.57
9	28.6	4.26	3.23	1.32	2.33
10	29.1	4.05	3.13	1.29	2.12
11	28.1	3.69	2.90	1.27	1.94
12	27.0	3.44	2.73	1.26	1.77
13	26.5	3.21	2.58	1.24	1.65
14	25.7	3.04	2.46	1.23	1.56

TABLE 3. Boundary layer bulk and integral properties, with C_f obtained using Fernholz & Finley (1996) correlation; see also table 1.

on the relation governing the location of the peak: either $u_{II}^{2+} = 0.42\ln(Re_\tau) + 2.82$, or $u_{II}^{2+} = 0.63\ln(Re_\tau) + 0.33$. Figure 5 shows that these relations are in generally good agreement with the data, although our analysis gives slightly different curve fits ($u_{II}^{2+} = 0.49\ln(Re_\tau) + 1.7$ in pipes and $u_{II}^{2+} = 0.47\ln(Re_\tau) + 2.0$ in boundary layers). The data broadly support the hypothesis of Pullin *et al.* that at the limit of infinite Reynolds number the wall-normal turbulent transport of turbulent energy declines and the turbulence is asymptotically attenuated across the whole outer layer. Hence, with increasing Reynolds number, the locations of the inner peak (at constant y^+) and the outer peak (varying as $\ln Re_\tau$) are both moving closer to the wall in physical coordinates, and so the asymptotic state of the wall layer is a slip-flow bounded by a vortex sheet at the wall (Pullin *et al.* 2013).

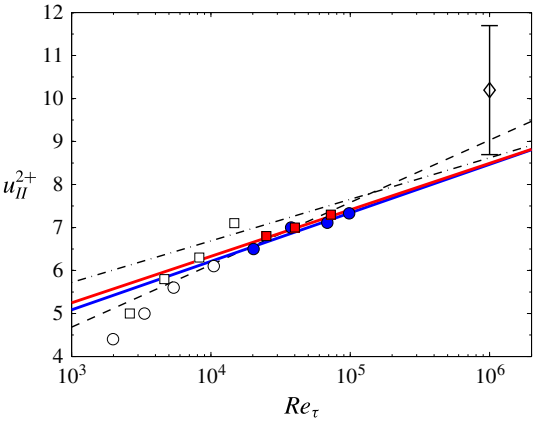

FIGURE 5. (Colour online) Magnitudes of the outer peak in u^{2+}: □, boundary layer; ○, pipe; filled symbols, $Re_\tau > 20\,000$; ◇, atmospheric boundary layer (Metzger, McKeon & Holmes 2007); - - - -, $u_{II}^{2+} = 0.63\ln(Re_\tau) + 0.33$ (Pullin, Inoue & Saito 2013); $-\cdot-\cdot-$, $u_{II}^{2+} = 0.42\ln(Re_\tau) + 2.82$ (Pullin *et al.* 2013); ——, best fit to pipe data, given by $u_{II}^{2+} = 0.49\ln(Re_\tau) + 1.7$; ——, best fit to boundary layer data, given by $u_{II}^{2+} = 0.47\ln(Re_\tau) + 2.0$.

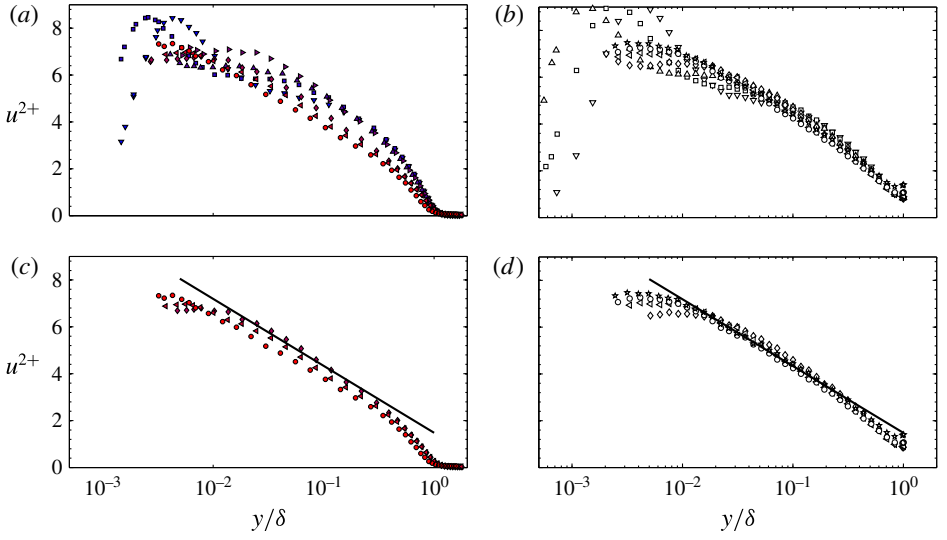

FIGURE 6. Variance profiles in outer coordinates: (*a*,*c*) boundary layer; (*b*,*d*) pipe. (*a*,*b*) All Re_τ; (*c*,*d*) data for $Re_\tau \geqslant 20\,000$ and $y^+ \geqslant 100$. Symbols as given in tables 1 and 2. Solid line, (1.2) with $A_1 = 1.24$ and $B_1 = 1.48$.

Figure 6 shows that in outer coordinates the variances do not collapse as well in boundary layers as they do in pipes, and a clear trend with increasing Reynolds numbers can be observed, especially at the lower Reynolds numbers. The mixed scaling $(u_\tau U_\infty)^{0.5}$, introduced for boundary layers by DeGraaff & Eaton (2000), did not noticeably improve the collapse, and so it was not pursued further.

For $Re_\tau > 20\,000$, the logarithmic behaviour described by (1.2) is observed in the boundary layer profiles for $y^+ \gtrsim 400$. This logarithmic behaviour can be seen more

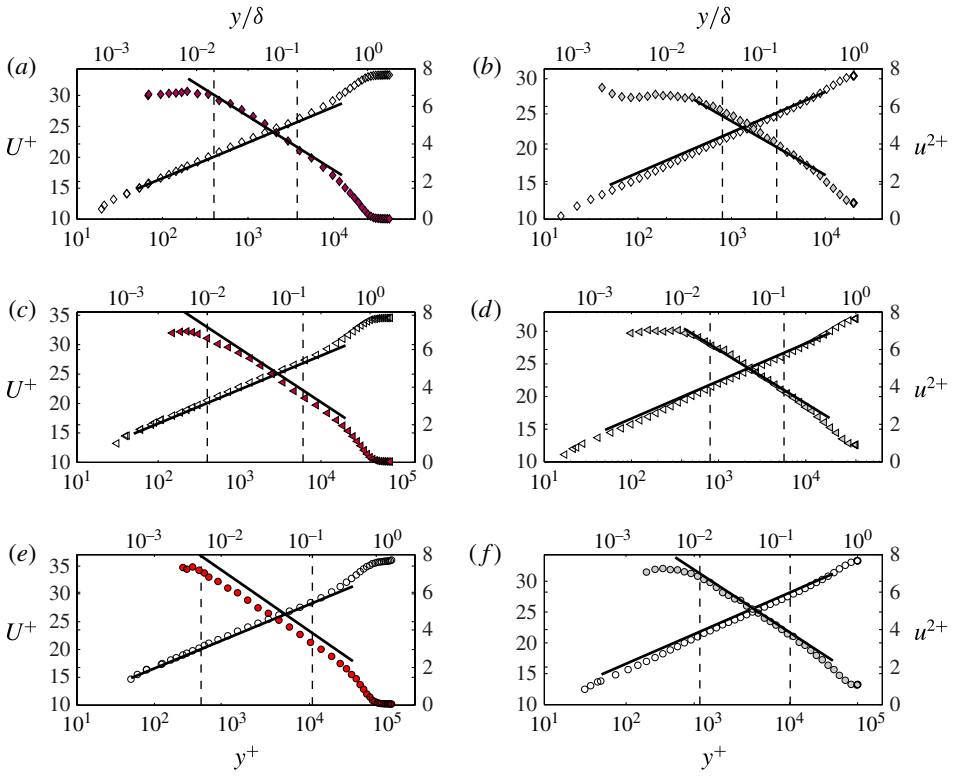

FIGURE 7. Mean velocity profiles (empty symbols) and turbulence intensities (filled symbols) for $Re_\tau \approx 20\,000$ (*a*,*b*), $Re_\tau \approx 40\,000$ (*c*,*d*), $Re_\tau \approx 70\,000$ (*e*,*f*) in the boundary layer (*a*,*c*,*e*) and the pipe (*b*,*d*,*f*). Symbols as given in tables 1 and 2. Lines: - - - -, limits of logarithmic region ($y^+ = 400$ and $y^+ = 0.15Re_\tau$ for the boundary layer, $y^+ = 800$ and $y^+ = 0.15Re_\tau$ for the pipe); ——, (1.1) with $\kappa = 0.40$, $B = 5.1$, and (1.2) with $A_1 = 1.24$, $B_1 = 1.48$.

clearly when the data are restricted to $Re_\tau > 20\,000$ and $y^+ > 100$. The Townsend–Perry constant $A_1 = 1.24$ and additive constant $B_1 = 1.48$ were taken from the results in pipe flow (Hultmark *et al.* 2013). The slope appears to be very similar in boundary layer and pipe flows, as found by Marusic *et al.* (2013) (who used $A_1 = 1.26$), but for boundary layers there seems to be some variation with Reynolds number in the additive constant. The uncertainty limits on these constants are unknown at present.

3.3. *Logarithmic regions in the mean and the variance*

Profiles of the mean velocity and the variances are shown cross-plotted together in figure 7. The dashed lines correspond to $y^+ = 400$ and $y/\delta = 0.15$ in the boundary layer, and $y^+ = 800$ and $y/\delta = 0.15$ in the pipe. Both the mean velocity and the variances follow a logarithmic behaviour within these limits, but the mean velocity in the boundary layer case seems to follow a logarithmic variation down to $y^+ \approx 100$. This result indicates the presence of an intermediate range below $y^+ \approx 400$ in boundary layers, and below $y^+ \approx 800$ in pipes, where the boundary layer variances deviate from the logarithmic behaviour in a manner very similar to that described in Hultmark (2012) for pipe flows. This region corresponds approximately to the

Case	Pipe		Boundary layer		Symbol
$Re_\tau \approx$	Re_τ	ℓ^+	Re_τ	ℓ^+	
3×10^3	3 334	3.1	2 622	5.8	▼
5×10^3	5 412	5.0	4 635	10	■
10×10^3	10 481	9.7	8 261	17	▲
20×10^3	20 250	18.8	25 062	29	♦
40×10^3	37 690	35.0	40 053	47	◀
70×10^3	68 371	31.7	72 526	75	●

TABLE 4. Cases chosen for comparing boundary layer (current data) and pipe flow (Hultmark *et al.* 2013).

mesolayer described by Afzal (1982, 1984), George & Castillo (1997), Sreenivasan & Sahay (1997), Wosnik, Castillo & George (2000) and Wei *et al.* (2005) in boundary layers, and the power law region described by McKeon *et al.* (2004) in pipes. George & Castillo (1997) suggested that in this region the mean velocity has reached a seemingly logarithmic behaviour but the effects of viscosity are still evident in the behaviour of the turbulent stress terms. Wei *et al.* (2005) identified the mesolayer with the region where the stress gradients are close to zero, and the viscous force balances the pressure force in pipe flow or the mean advection in the turbulent boundary layer. The present results are at a sufficiently high Reynolds number to distinguish the mesolayer clearly from the logarithmic region where all viscous effects are negligible, but a more precise statement needs a consideration of the spectral behaviour, which is given by Vallikivi *et al.* (2015).

3.4. *Higher-order moments*

We now consider the behaviour of the higher-order moments of the streamwise velocity fluctuations (up to 10th order). Because no established correction for spatial filtering on higher-order moments exists, data with more than 5 % spatial filtering on the variances, as indicated by the spatial filtering correction, were excluded from the analysis.

To make direct comparisons between boundary layer and pipe flows, six cases with matching Reynolds numbers were chosen: cases 1–3 and 5–7 given in table 1 for the boundary layer, and cases 1–6 given in table 2 for the pipe. These cases correspond to $Re_\tau \approx$ 3000, 5000, 10 000, 20 000, 40 000, and 70 000, and they are summarized in table 4. The higher-order moments for the pipe are reported here for the first time, although they are based on the data collected by Hultmark *et al.* (2013).

Figure 8 shows, for a representative boundary layer case, the probability density function $P(u)$ (p.d.f.), and the premultiplied probability density function $u^{2p}P(u)$, where $2p = [2, 6, 10]$ indicates the pth even moment. Each moment is the area under the corresponding curve, and the data appear to be statistically converged. We see a clear deviation around the maximum value in the p.d.f. from a Gaussian behaviour, as well as deviations from symmetry in the premultiplied p.d.f.s.

The skewness $S = \langle u^3 \rangle / \langle u^2 \rangle^{3/2}$ is shown in figure 9. Both flows exhibit a very similar behaviour, with the skewness slightly positive near the wall for $y^+ < 200$ and becoming negative further away from the wall. For the boundary layer, the skewness is well collapsed in inner coordinates over the region $100 < y^+ < 0.15Re_\tau$, and we see all profiles change sign at $y^+ \approx 200$ and reach a value of $S \approx -0.1$ before becoming more

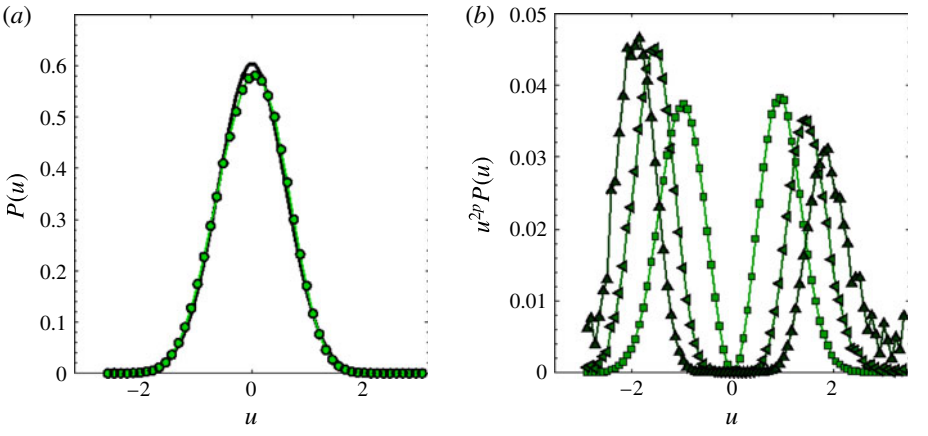

FIGURE 8. (Colour online) Probability density functions for the boundary layer at $Re_\tau = 70\,000$, $y^+ = 800$. (*a*) ●, $P(u)$; ——, Gaussian distribution. (*b*) $u^{2p}P(u)$; ■, $2p = 2$; ◀, $2p = 6$; ▲, $2p = 10$.

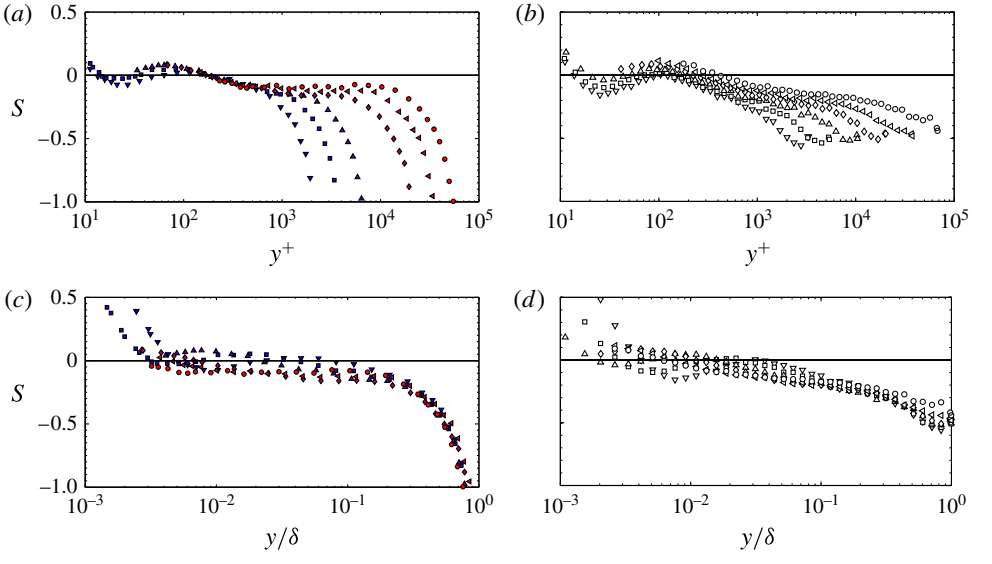

FIGURE 9. Skewness in inner coordinates (*a*,*b*) and outer coordinates (*c*,*d*) for cases given in table 4. (*a*,*c*) Boundary layer; (*b*,*d*) pipe.

negative in the wake, where they collapse well in outer coordinates. In contrast, the pipe flow profiles show a small Reynolds number dependence over the log region, and the collapse in the wake region in terms of outer layer coordinates is not as clean as that seen in the boundary layer data.

The kurtosis $K = \langle u^4 \rangle / \langle u^2 \rangle^2$ is shown in figure 10. Again, the behaviour for the two flows is very similar, with perhaps some small dependence on the Reynolds number in the outer region (although this could also be the result of some unresolved spatial filtering effects).

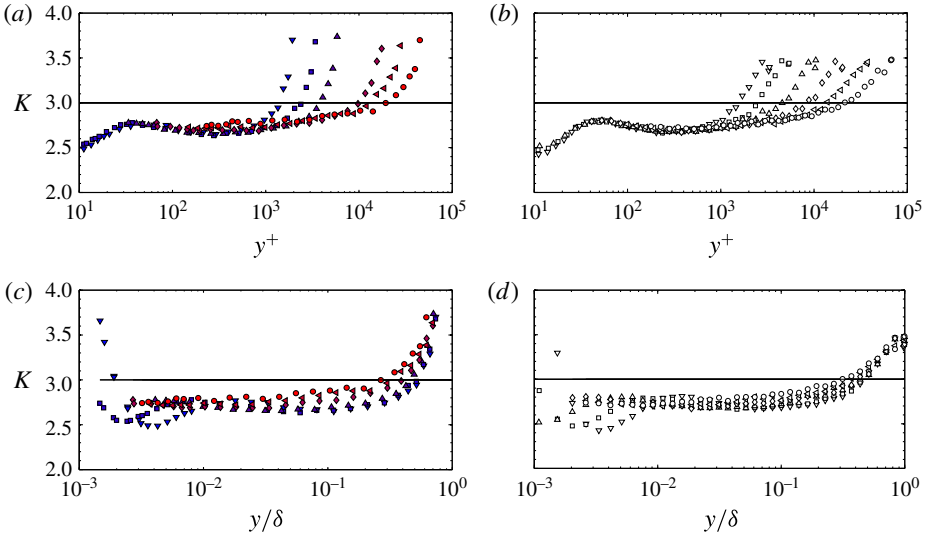

FIGURE 10. Kurtosis in inner coordinates (*a*,*b*) and outer coordinates (*c*,*d*) for cases given in table 4. (*a*,*c*) Boundary layer; (*b*,*d*) pipe.

The pth roots of the pth even moments $\langle (u^+)^{2p} \rangle^{1/p}$ are shown in figure 11 for $2p = 2$, 6, and 10 (the data for $2p = 4$, 8, and 12 show the same trends). In inner coordinates, the behaviour is qualitatively similar to that seen in the variances, with an inner peak at about $y^+ = 15$ that is either increasing very slowly with Reynolds number or not at all, a blending region over the range $30 < y^+ < 300$, followed by a logarithmic region. The results from the boundary layer and the pipe agree well throughout most of the flow, with the only differences appearing in the outer layer due to the different outer boundary conditions, as expected. Some minor differences can also be seen in the near-wall region, around $y^+ \approx 15$, where the pipe flow displays a slightly higher peak value, possibly due to smaller spatial filtering effects since ℓ^+ is smaller for the pipe than the boundary layer (see table 4). Finally, it appears that the inner limit of the logarithmic range for pipes occurs at higher values of y^+ than in boundary layers, similar to what was observed for the variances.

Figure 11 also displays the data in outer coordinates for the three highest Reynolds numbers ($Re_\tau \geqslant 20\,000$). As seen in the variances, the higher moments show good agreement between boundary layer and pipe flows. With increasing moment, the agreement improves, and the range of logarithmic behaviour increases.

The constants A_p and B_p in (1.3) were found by regression fit to each profile, that is, separately for each flow, Reynolds number, and moment. To test the consequences of choosing a particular range for the curve fit, different ranges were used for fitting, with the inner limit varying as $y^+_{min} = [3Re_\tau^{0.5}; 200; 400; 600; 800]$ while keeping a constant outer limit at $(y/\delta)_{max} = 0.15$ (the results were not sensitive to reasonable variations in the outer limit). A minimum of four points in each profile were used for determining the constants, otherwise the profile was discarded as not having a sufficiently extensive logarithmic region.

The variation of the slope A_p with p is shown in figure 12. For Gaussian statistics, A_p would vary as $A_1[(2p-1)!!]^{1/p}$, where A_1 is the Townsend–Perry constant and !! denotes double factorial. It is evident that for boundary layer and pipe flows all the constants have a sub-Gaussian behaviour, as observed by Meneveau & Marusic (2013)

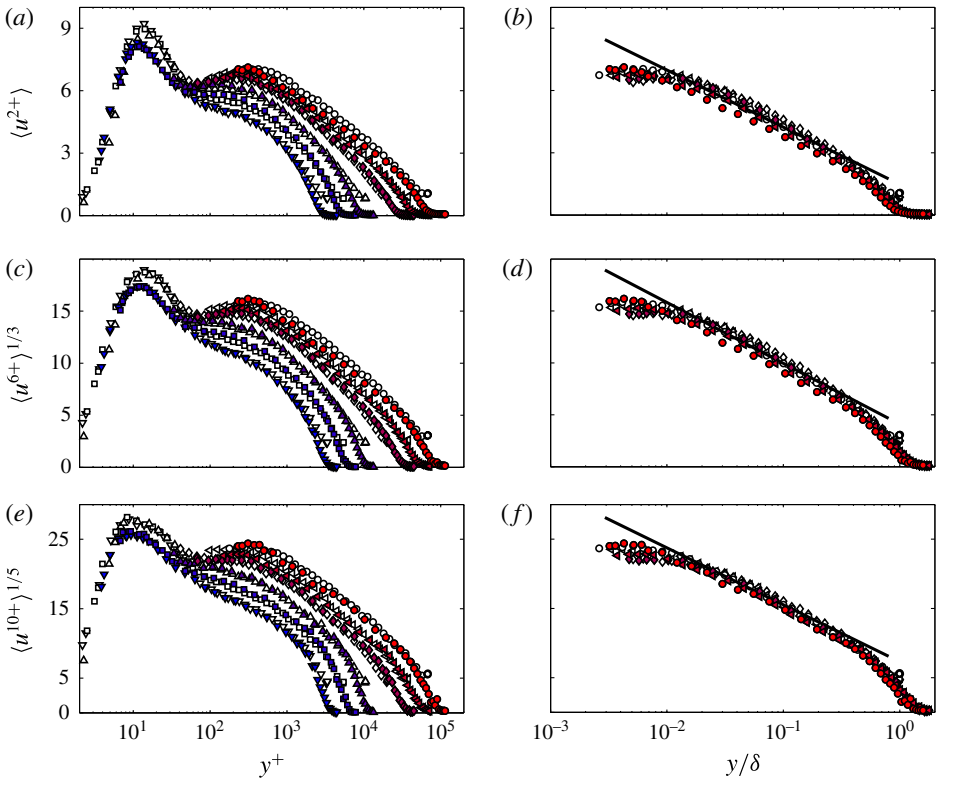

FIGURE 11. Higher-order even moments $2p = 2$, 6, and 10 for boundary layer (filled symbols) and pipe flow (empty symbols). Data in inner coordinates (*a*,*c*,*e*) for all cases given in table 4. Same data in outer coordinates (*b*,*d*,*f*) for $Re_\tau \geqslant 20\,000$ and $y^+ > 100$. Solid line, (1.3) with A_p and B_p derived from the pipe flow profile at $Re_\tau = 70\,000$ (where $A_p = [1.13; 2.48; 3.44]$ and $B_p = [1.17; 3.31; 6.73]$ accordingly).

for boundary layers at lower Reynolds numbers. For smaller y^+_{min} values, there is a clear Reynolds number dependence in A_p between cases, as well as a dependence on y^+_{min}. For both flows, A_p was found to become independent of Re_τ for $y^+_{min} \gtrsim 400$. The limit $y^+_{min} = 3Re_\tau^{0.5}$ used by Meneveau & Marusic (2013) underestimates the inner limit at low Re_τ while overestimating it at high Re_τ, and so it appears that either a constant inner limit or one with a very weak Re_τ dependence is more appropriate for both flows. A good representation of the asymptotic value of the slope is given empirically by $A_p \sim A_1(2p-1)^{1/2}$ for both pipe and boundary layer ($A_1 = 1.24$, as before).

It appears that if a large enough value of y^+_{min} is chosen, A_p is independent of Reynolds number in pipe and boundary layer flows. The only outlier, the highest Reynolds number case for the boundary layer, has a slightly lower value of A_p, but this could be due to experimental error, which is expected to be greatest at the highest Reynolds number.

The behaviour of the additive constant B_p is more difficult to establish, due to its high sensitivity to the magnitude of the moments. In pipes the constant appears to be independent of Reynolds number, whereas in boundary layers a weak dependence is observed in most cases. In contrast, Meneveau & Marusic (2013) found a much stronger dependence, possibly caused by using $3Re_\tau^{0.5}$ as the inner limit on the curve

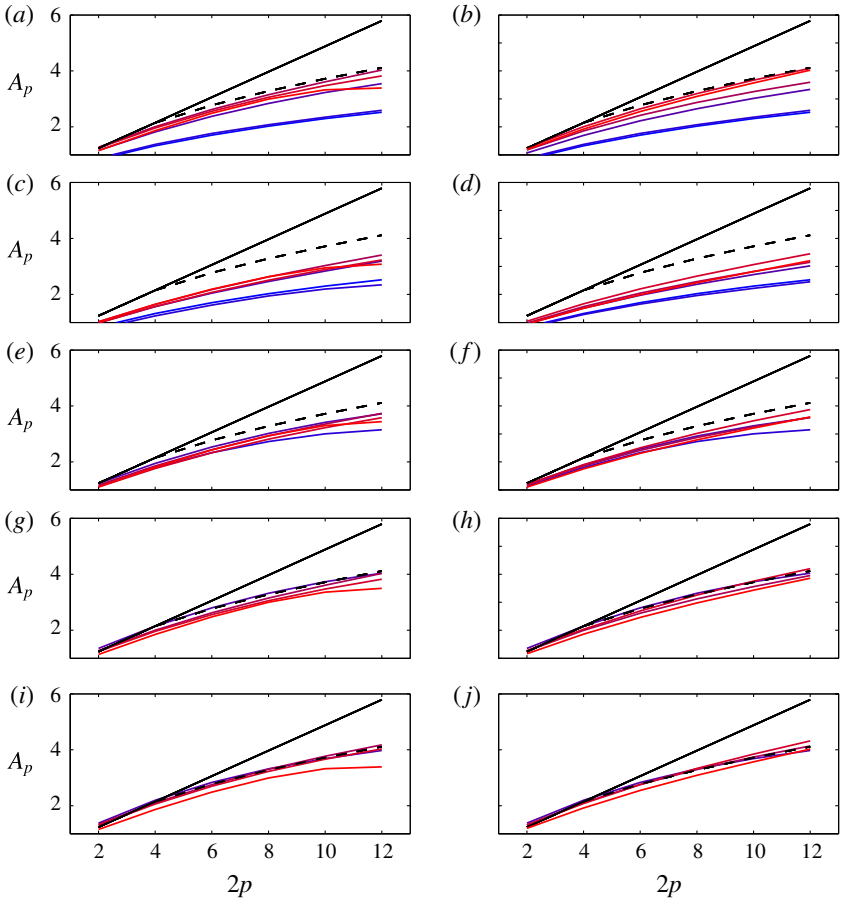

FIGURE 12. Constant A_p for even moments $2p$, for the fitting range $y^+ = [y^+_{min}, 0.15Re_\tau]$. Left: boundary layer; right: pipe. Line colors given in table 4. ——, expected Gaussian variation $A_p = A_1[(2p-1)!!]^{1/p}$; - - - -, empirical fit $A_p = A_1(2p-1)^{1/2}$.

fit. Interestingly, for the current data set B_p reached a constant value for the three highest Reynolds number cases when $y^+_{min} \geqslant 600$ was used as inner limit, which could suggest that high-order moments are still affected by viscosity for smaller y^+. However, these trends are probably within experimental error, and no strong conclusions can be made.

4. Conclusions

Zero-pressure-gradient turbulent boundary layer measurements for $2600 < Re_\tau < 72\,500$ were compared with previously acquired pipe flow data at similar Reynolds numbers. These Reynolds numbers covered a sufficient range to enable identification of some apparently asymptotic trends. For $Re_\tau \geqslant 20\,000$, the mean velocity and variance profiles showed extended logarithmic regions, with very similar constants in both flows. The two logarithmic regions coincide over the region $400 \lesssim y^+ \lesssim 0.15Re_\tau$. The inner limit may not be a perfect constant but may be subject to a weak Reynolds number dependence (certainly less than $Re_\tau^{0.5}$), and it is further explored by Vallikivi *et al.* (2015) when considering the spectral behaviour.

Higher-order even moments also show a logarithmic behaviour over the same physical space as the mean velocity and the variances, and the slope of the line appears to become independent of Reynolds number for the same region, defined by $400 \lesssim y^+ \lesssim 0.15Re_\tau$ for both boundary layer and pipe flows. These bounds define a Reynolds number of $Re_\tau \approx 27\,000$ where this region extends over a decade in y^+, underlining the need to obtain data at Reynolds numbers comparable to those obtained here if one wants to study scaling behaviours.

Acknowledgements

The authors would like to thank B. McKeon and acknowledge J. Allen for their help in the design and construction of the flat-plate apparatus and the pressure gradient blister, G. Kunkel, R. Echols and S. Bailey for conducting preliminary tests, and B. Ganapathisubramani and W. K. George for many insightful discussions and suggestions. This work was made possible by support received through ONR grant N00014-13-1-0174, program manager R. Joslin, and NSF grant CBET-1064257, program managers H. Winter and D. Papavassiliou.

REFERENCES

AFZAL, N. 1982 Fully developed turbulent flow in a pipe: an intermediate layer. *Ing.-Arch.* **52**, 355–377.

AFZAL, N. 1984 Mesolayer theory for turbulent flows. *AIAA J.* **22**, 437–439.

BAILEY, S. C. C., HULTMARK, M., MONTY, J. P., ALFREDSSON, P. H., CHONG, M. S., DUNCAN, R. D., FRANSSON, J. H. M., HUTCHINS, N., MARUSIC, I., MCKEON, B. J., NAGIB, H. M., ÖRLÜ, R., SEGALINI, A., SMITS, A. J. & VINUESA, R. 2013 Obtaining accurate mean velocity measurements in high Reynolds number turbulent boundary layers using Pitot tubes. *J. Fluid Mech.* **715**, 642–670.

BAILEY, S. C. C., KUNKEL, G. J., HULTMARK, M., VALLIKIVI, M., HILL, J. P., MEYER, K. A., TSAY, C., ARNOLD, C. B. & SMITS, A. J. 2010 Turbulence measurements using a nanoscale thermal anemometry probe. *J. Fluid Mech.* **663**, 160–179.

BAILEY, S. C. C., VALLIKIVI, M., HULTMARK, M. & SMITS, A. J. 2014 Estimating the value of von Kármán's constant in turbulent pipe flow. *J. Fluid Mech.* **749**, 79–98.

CLAUSER, F. H. 1956 The turbulent boundary layer. *Adv. Mech.* **4**, 1–51.

COLES, D. E. 1956 The law of the wake in the turbulent boundary layer. *J. Fluid Mech.* **1**, 191–226.

DEGRAAFF, D. B. & EATON, J. K. 2000 Reynolds-number scaling of the flat-plate turbulent boundary layer. *J. Fluid Mech.* **422**, 319–346.

FERNHOLZ, H. H. & FINLEY, P. J. 1996 The incompressible zero-pressure-gradient turbulent boundary layer: an assessment of the data. *Prog. Aerosp. Sci.* **32**, 245–311.

GEORGE, W. K. & CASTILLO, L. 1997 Zero-pressure-gradient turbulent boundary layer. *Appl. Mech. Rev.* **50**, 689–729.

HULTMARK, M. 2012 A theory for the streamwise turbulent fluctuations in high Reynolds number pipe flow. *J. Fluid Mech.* **707**, 575–584.

HULTMARK, M. & SMITS, A. J. 2010 Temperature corrections for constant temperature and constant current hot-wire anemometers. *Meas. Sci. Technol.* **21**, 105404.

HULTMARK, M., VALLIKIVI, M., BAILEY, S. C. C. & SMITS, A. J. 2012 Turbulent pipe flow at extreme Reynolds numbers. *Phys. Rev. Lett.* **108** (9), 1–5.

HULTMARK, M., VALLIKIVI, M., BAILEY, S. C. C. & SMITS, A. J. 2013 Logarithmic scaling of turbulence in smooth- and rough-wall pipe flow. *J. Fluid Mech.* **728**, 376–395.

HUTCHINS, N., CHAUHAN, K. A., MARUSIC, I., MONTY, J. & KLEWICKI, J. 2012 Towards reconciling the large-scale structure of turbulent boundary layers in the atmosphere and laboratory. *Boundary-Layer Meteorol.* **145**, 273–306.

JIMÉNEZ, J. M., HULTMARK, M. & SMITS, A. J. 2010 The intermediate wake of a body of revolution at high Reynolds numbers. *J. Fluid Mech.* **659**, 516–539.

MACMILLAN, F. A. 1957 Experiments on Pitot tubes in shear flow. No. 3028 Ministry of Supply, Aeronautical Research Council.

MARUSIC, I., MCKEON, B. J., MONKEWITZ, P. A., NAGIB, H. M., SMITS, A. J. & SREENIVASAN, K. R. 2010 Wall-bounded turbulent flows: recent advances and key issues. *Phys. Fluids* **22**, 065103.

MARUSIC, I., MONTY, J. P., HULTMARK, M. & SMITS, A. J. 2013 On the logarithmic region in wall turbulence. *J. Fluid Mech.* **716**, R3,1–3.

MATHIS, R., HUTCHINS, N. & MARUSIC, I. 2009 Large-scale amplitude modulation of the small-scale structures in turbulent boundary layers. *J. Fluid Mech.* **628**, 311–337.

MCKEON, B. J., LI, J., JIANG, W., MORRISON, J. F. & SMITS, A. J. 2003 Pitot probe corrections in fully developed turbulent pipe flow. *Meas. Sci. Technol.* **14** (8), 1449–1458.

MCKEON, B. J., LI, J., JIANG, W., MORRISON, J. F. & SMITS, A. J. 2004 Further observations on the mean velocity distribution in fully developed pipe flow. *J. Fluid Mech.* **501**, 135–147.

MCKEON, B. J. & SMITS, A. J. 2002 Static pressure correction in high Reynolds number fully developed turbulent pipe flow. *Meas. Sci. Technol.* **13**, 1608–1614.

MENEVEAU, C. & MARUSIC, I. 2013 Generalized logarithmic law for high-order moments in turbulent boundary layers. *J. Fluid Mech.* **719**, R1.

METZGER, M., MCKEON, B. J. & HOLMES, H. 2007 The near-neutral atmospheric surface layer: turbulence and non-stationarity. *Phil. Trans. R. Soc. Lond.* A **365** (1852), 859–876.

MILLIKAN, C. B. 1938 A critical discussion of turbulent flows in channels and circular tubes. In *Proceedings of the fifth International Congress for Applied Mechanics*, pp. 386–392. Wiley/Chapman and Hall.

NAGIB, H. M., CHAUHAN, K. A. & MONKEWITZ, P. A. 2007 Approach to an asymptotic state for zero pressure gradient turbulent boundary layers. *Phil. Trans. R. Soc. Lond.* A **365** (1852), 755–770.

ÖSTERLUND, J. M., JOHANSSON, A. V., NAGIB, H. M. & HITES, M. H. 2000 A note on the overlap region in turbulent boundary layers. *Phys. Fluids* **12** (1), 1–4.

PATEL, V. C. 1965 Calibration of the Preston tube and limitations on its use in pressure gradients. *J. Fluid Mech.* **23**, 185–208.

PERRY, A. E., HENBEST, S. M. & CHONG, M. S. 1986 A theoretical and experimental study of wall turbulence. *J. Fluid Mech.* **165**, 163–199.

PULLIN, D. I., INOUE, M. & SAITO, N. 2013 On the asymptotic state of high Reynolds number, smooth-wall turbulent flows. *Phys. Fluids* **25** (1), 105116.

ROSENBERG, B. J., HULTMARK, M., VALLIKIVI, M., BAILEY, S. C. C. & SMITS, A. J. 2013 Turbulence spectra in smooth- and rough-wall pipe flow at extreme Reynolds numbers. *J. Fluid Mech.* **731**, 46–63.

SMITS, A. J. & MARUSIC, I. 2013 Wall-bounded turbulence. *Phys. Today* 25–30.

SMITS, A. J., MCKEON, B. J. & MARUSIC, I. 2011*a* High Reynolds number wall turbulence. *Annu. Rev. Fluid Mech.* **43**, 353–375.

SMITS, A. J., MONTY, J., HULTMARK, M., BAILEY, S. C. C., HUTCHINS, M. & MARUSIC, I. 2011*b* Spatial resolution correction for turbulence measurements. *J. Fluid Mech.* **676**, 41–53.

SREENIVASAN, K. R. & SAHAY, A. 1997 The persistence of viscous effects in the overlap region and the mean velocity in turbulent pipe and channel flows. In *Self-Sustaining Mechanisms of Wall Turbulence* (ed. R. Panton), pp. 253–272. Comp. Mech. Publ.

TOWNSEND, A. A. 1976 *The Structure of Turbulent Shear Flow*. Cambridge University Press.

VALLIKIVI, M. 2014 Wall-bounded turbulence at high Reynolds numbers. PhD thesis, Princeton University.

VALLIKIVI, M., GANAPATHISUBRAMANI, B. & SMITS, A. J. 2015 Spectra in boundary layers and pipes at very high Reynolds numbers. *J. Fluid Mech.* **771**, 303–326.

VALLIKIVI, M., HULTMARK, M., BAILEY, S. C. C. & SMITS, A. J. 2011 Turbulence measurements in pipe flow using a nano-scale thermal anemometry probe. *Exp. Fluids* **51**, 1521–1527.

VALLIKIVI, M., HULTMARK, M. & SMITS, A. J. 2013 The scaling of very high Reynolds number turbulent boundary layers. In *8th International Symposium on Turbulence and Shear Flow Phenomena*, *Poitiers, France*.

VALLIKIVI, M. & SMITS, A. J. 2014 Fabrication and characterization of a novel nano-scale thermal anemometry probe. *J. Microelectromech. Syst.* **23** (4), 899–907.

WEI, T., FIFE, P., KLEWICKI, J. C. & MCMURTRY, P. 2005 Properties of the mean momentum balance in turbulent boundary layer, pipe and channel flows. *J. Fluid Mech.* **522**, 303–327.

WINKEL, E. S., CUTBIRTH, J. M., CECCIO, S. L., PERLIN, M. & DOWLING, D. R. 2012 Turbulence profiles from a smooth flat-plate turbulent boundary layer at high Reynolds number. *Exp. Therm. Fluid Sci.* **40**, 140–149.

WINTER, K. G. & GAUDET, L. 1970 Turbulent boundary-layer studies at high Reynolds numbers at Mach numbers between 0.2 and 2.8. R & M No. 3712. Aeronautical Research Council, Ministry of Aviation Supply, Royal Aircraft Establishment, RAE.

WOSNIK, M., CASTILLO, L. & GEORGE, W. K. 2000 A theory for turbulent pipe and channel flows. *J. Fluid Mech.* **421**, 115–145.

ZAGAROLA, M. V. & SMITS, A. J. 1998 Mean-flow scaling of turbulent pipe flow. *J. Fluid Mech.* **373**, 33–79.

ZAGAROLA, M. V., WILLIAMS, D. R. & SMITS, A. J. 2001 Calibration of the Preston probe for high Reynolds number flows. *Meas. Sci. Technol.* **12**, 495–501.